Title

Immunoediting role for major vault protein in apoptotic signaling induced by bacterial N-acyl homoserine lactones

Journal

Proceedings of the National Academy of Sciences of the United States of America, 118(12)

ISSN

0027-8424

Authors

Rayo, Josep
Gregor, Rachel
Jacob, Nicholas T
et al.

Publication Date

2021-03-23

DOI

10.1073/pnas.2012529118

Peer reviewed

Immunoediting role for major vault protein in apoptotic signaling induced by bacterial *N*-acyl homoserine lactones

Josep Rayo[a,1], Rachel Gregor[a,1], Nicholas T. Jacob[b,c,d,1], Rambabu Dandela[a], Luba Dubinsky[a], Alex Yashkin[a], Alexander Aranovich[a], Manikandan Thangaraj[a], Orna Ernst[e], Eran Barash[f], Sergey Malitsky[g], Bogdan I. Florea[h], Bastiaan P. Krom[i], Erik A. C. Wiemer[j], Valerie A. Kickhoefer[k], Leonard H. Rome[k], John C. Mathison[b], Gunnar F. Kaufmann[c,d], Herman S. Overkleeft[h], Benjamin F. Cravatt[l], Tsaffrir Zor[e], Kim D. Janda[b,c,d], Richard J. Ulevitch[b], Vladimir V. Kravchenko[b,2], and Michael M. Meijler[a,2]

[a]Department of Chemistry and the National Institute for Biotechnology in the Negev, Ben-Gurion University of the Negev, Be'er Sheva 8410501, Israel; [b]Department of Immunology and Microbial Sciences, The Scripps Research Institute, La Jolla, CA 92037; [c]Department of Chemistry, The Skaggs Institute for Chemical Biology, The Scripps Research Institute, La Jolla, CA 92037; [d]The Worm Institute of Research and Medicine, The Scripps Research Institute, La Jolla, CA92037; [e]Department of Biochemistry & Molecular Biology, Life Sciences Institute, Tel Aviv University, Tel Aviv 69978, Israel; [f]Department of Computer Science, Ben-Gurion University of the Negev, Be'er Sheva 8410501, Israel; [g]Life Sciences Core Facilities, Weizmann Institute of Science, Rehovot 7610001, Israel; [h]Department of Bio-organic Synthesis, Leiden Institute of Chemistry, Leiden University, 2333 ZA Leiden, The Netherlands; [i]Department of Preventive Dentistry, Academic Centre for Dentistry, 1081 LA Amsterdam, The Netherlands; [j]Department of Medical Oncology, Erasmus Medical Center Cancer Institute, Erasmus University Medical Center, 3015 GD Rotterdam, The Netherlands; [k]Department of Biological Chemistry, David Geffen School of Medicine at University of California Los Angeles, Los Angeles, CA 90095; and [l]Department of Chemical Physiology, The Scripps Research Institute, La Jolla, CA 92037

Edited by Ralph R. Isberg, Tufts University School of Medicine, Boston, MA, and approved December 31, 2020 (received for review June 22, 2020)

The major vault protein (MVP) mediates diverse cellular responses, including cancer cell resistance to chemotherapy and protection against inflammatory responses to *Pseudomonas aeruginosa*. Here, we report the use of photoactive probes to identify MVP as a target of the *N*-(3-oxo-dodecanoyl) homoserine lactone (C12), a quorum sensing signal of certain proteobacteria including *P. aeruginosa*. A treatment of normal and cancer cells with C12 or other *N*-acyl homoserine lactones (AHLs) results in rapid translocation of MVP into lipid raft (LR) membrane fractions. Like AHLs, inflammatory stimuli also induce LR-localization of MVP, but the C12 stimulation reprograms (functionalizes) bioactivity of the plasma membrane by recruiting death receptors, their apoptotic adaptors, and caspase-8 into LR. These functionalized membranes control AHL-induced signaling processes, in that MVP adjusts the protein kinase p38 pathway to attenuate programmed cell death. Since MVP is the structural core of large particles termed vaults, our findings suggest a mechanism in which MVP vaults act as sentinels that fine-tune inflammation-activated processes such as apoptotic signaling mediated by immunosurveillance cytokines including tumor necrosis factor-related apoptosis inducing ligand (TRAIL).

bacterial signaling | immunoediting | cross-kingdom communication | immunosurveillance

Cancer immunoediting is a dynamic process composed of three phases—elimination, equilibrium, and escape (1, 2). According to this hypothesis, if immunosurveillance effectors fail to mediate apoptosis in nascent neoplasm, the transformed cells enter the equilibrium phase where they are either maintained chronically or "edited" immunologically, thereby producing new populations of tumor variants in the escape phase (2). The inflammatory microenvironment—including microbial metabolites such as lipopolysaccharides (LPS) and proinflammatory cytokines such as tumor necrosis factor (TNF)—affects signaling processes in cells experiencing any of the three phases of cancer immunoediting (2–6) and can promote the generation of tumor cells that are resistant to proapoptotic immunosurveillance factors, such as TNF-related apoptosis inducing ligand (TRAIL) (7–9). Of note, the resistance of tumor cells to TRAIL-induced apoptosis is overcome in the presence of Gram-negative bacteria, which produce *N*-acyl homoserine lactones (AHLs), such as C12 (10). The ability of AHLs to affect proapoptotic signaling in normal and transformed cells (10, 11) suggests a mechanism by which immunoediting processes are reprogramed in response to proteobacterial metabolites.

Results and Discussion

Previously, we developed a series of bifunctional photoactive probes of C12 for chemoproteomic profiling (*SI Appendix*, Fig. S1, compounds **6**, **7**, and **8**), of which P6 demonstrated agonistic characteristics equal to C12 in normal human bronchial epithelial (NHBE) cells (12). To identify C12-specific targets in human cells, we performed stable isotope labeling by amino acids (SILAC) experiments on NHBE cells treated with P6 or control

Significance

It has become clear that our immune system can significantly inhibit the growth of cancer cells, in a process that has been coined "cancer immunoediting." Based on this model, if the programmed cell death (apoptosis) mediated through immunosurveillance processes is not successful, the tumor cells may enter an equilibrium phase where they are either maintained or "edited" immunologically, leading to populations of tumor variants in the escape phase. Microbial factors have been found to affect cancer immunoediting. In this study we have identified a central player in these processes, called the major vault protein (MVP). Binding of certain bacterial signaling molecules to MVP strongly modulates apoptotic signaling, provoking new ideas and avenues to understand human-bacterial relationships and fight cancer.

Author contributions: J.R., R.G., N.T.J., A.Y., A.A., O.E., S.M., V.V.K., and M.M.M. designed research; J.R., R.G., N.T.J., L.D., A.Y., A.A., O.E., S.M., V.V.K., and M.M.M. performed research; J.R., R.G., R.D., L.D., A.Y., M.T., B.P.K., E.A.C.W., V.A.K., L.H.R., J.C.M., G.F.K., T.Z., K.D.J., R.J.U., V.V.K., and M.M.M. contributed new reagents/analytic tools; J.R., R.G., N.T.J., A.A., O.E., E.B., S.M., B.I.F., H.S.O., B.F.C., T.Z., V.V.K., and M.M.M. analyzed data; and J.R., R.G., V.V.K., and M.M.M. wrote the paper.

The authors declare no competing interest.

This article is a PNAS Direct Submission.

[1]J.R., R.G., and N.T.J. contributed equally to this work.

[2]To whom correspondence may be addressed. Email: vkrav@scripps.edu or meijler@bgu.ac.il.

This article contains supporting information online at https://www.pnas.org/lookup/suppl/doi:10.1073/pnas.2012529118/-/DCSupplemental.

Published March 15, 2021.

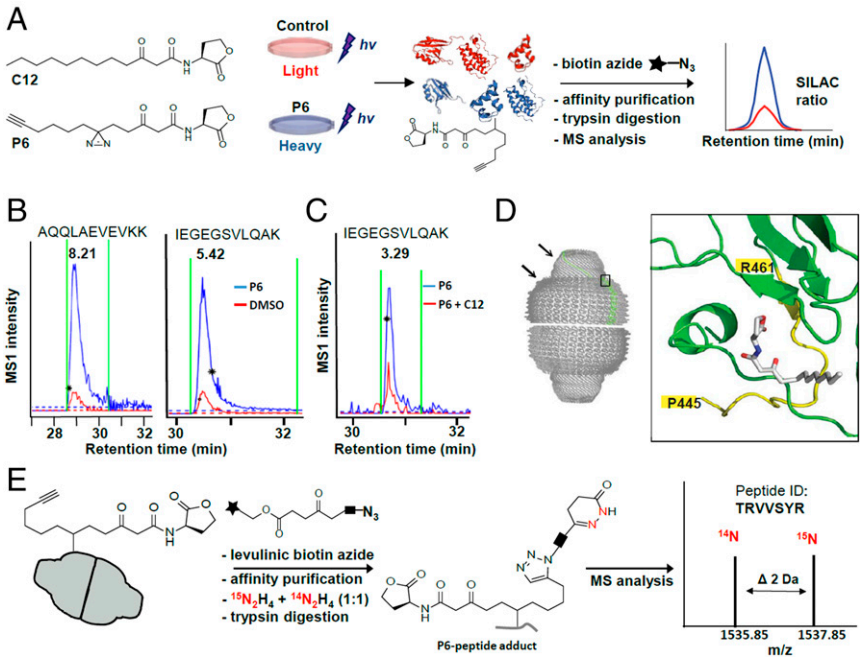

Fig. 1. Chemical proteomic analysis identifies MVP as a potential target of C12. (*A*) General scheme of the chemical proteomics strategy, utilizing the probe P6 (*Left*, *Bottom*). (*B*) Representative LC–MS profiles of identified MVP peptides. SILAC ratios and peptide sequences are shown on the top. (*C*) Representative example of a competition effect of C12 on P6-mediated MVP labeling. Labeling by the probe in the presence of the native molecule C12 (red) is reduced when compared to labeling with the probe alone (blue). (*D*) The left panel shows barrel-like structure of vault, with MVP unit marked in green; top and bottom arrows mark vault cap and shoulder regions, respectively. The right panel shows the results of in silico docking simulation of MVP-C12 interaction, suggesting C12 (white) localization in a close proximity to shoulder region of vault (yellow). (*E*) Representative example using the hydrazine (N_2H_4) cleavable levulinic linker for the identification of P6 peptide adducts from a vault labeling experiment. The *m/z* values for matched pair of light (^{14}N) and heavy (^{15}N) adducts identifying MVP peptide are shown, resulting in a characteristic doublet signal. Images and molecules shown in *A*, *D*, and *E* are not drawn to scale. For additional information relevant to experiments described above, see *SI Appendix*, Figs. S2–S4.

compounds (vehicle or C12), and after covalent labeling by ultraviolet (UV)-irradiation, followed by lysis, orthogonal conjugation with biotin azide, and affinity purification, the obtained proteome samples were analyzed by liquid chromatography tandem mass spectrometry (Fig. 1*A*). Among several P6-targeted proteins identified in these studies, the major vault protein (MVP)

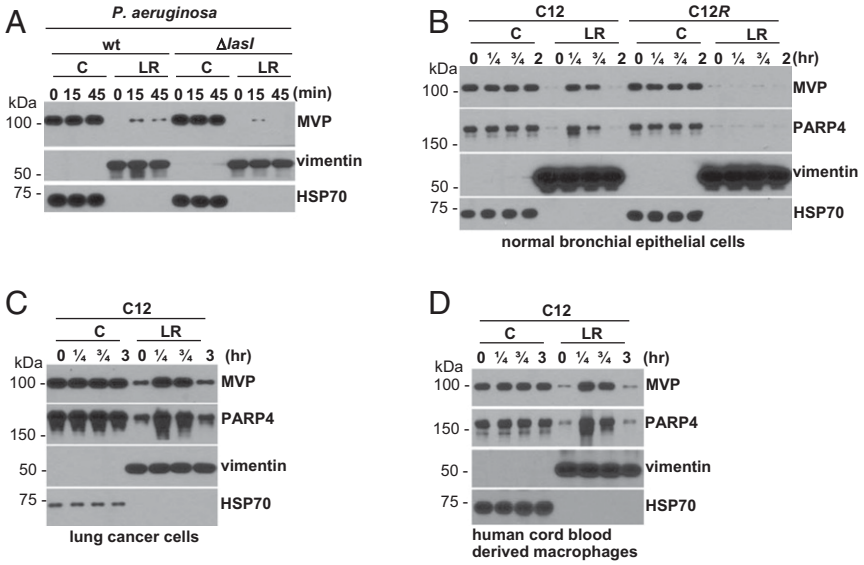

Fig. 2. C12-producing *P. aeruginosa* and C12 alone induce MVP translocation to LR fractions. (*A*) Comparison of NHBE cell responsiveness to *P. aeruginosa* wild type (wt) or *lasI* mutant (Δ*lasI*) by using WB analysis of cellular fractions containing cytosol (C) or LRs for expression of MVP, vimentin (a marker of LR fractions), and HSP70 (a marker of cytosol fraction). (*B*) NHBE cells were stimulated with C12 or its unnatural *R*-stereoisomer (C12R), and cellular samples were analyzed as in *A* as well as for expression of PARP4. (*C*, *D*) A549 lung cancer cell line (*C*) and normal human CBM (*D*) were stimulated with C12 and analyzed as indicated in *B*. For additional information relevant to experiments described above, see *SI Appendix*, Figs. S5 and S6.

consistently displayed high labeling ratios in comparison to controls (Fig. 1 *B* and *C* and *SI Appendix*, Fig. S2; all proteins that were identified using this methodology are listed in Dataset S1).

The evolutionarily conserved protein MVP is expressed as large, barrel-like particles termed vaults that are found in eukaryotes, including human cells (Fig. 1*D*) (13–16). Heterologous expression of MVP results in an assembly of vault particles, which are structurally indistinguishable from their naturally occurring counterparts (16–18). Therefore, in order to validate our cell-based proteomic findings, we examined whether our C12-based probe P6 targets recombinant human vaults. As expected, P6 labeled the recombinant vaults in a dose-dependent manner (*SI Appendix*, Fig. S3*A*). Importantly, P6 labeling of MVP was notably reduced in the presence of C12 (*SI Appendix*, Fig. S3*B*), indicating that both compounds interact with the vault in a similar manner. To further confirm these findings, the recombinant vault P6 adducts were additionally coupled with a biotinylated azide containing a levulinic acid-based cleavable linker. After streptavidin-based affinity purification, the P6-labeled peptides were released by cleaving the linker using an equimolar mixture of ^{15}N- and ^{14}N-hydrazine, yielding a characteristic doublet profile observed in subsequent mass spectrometry analysis (Fig. 1*E*). According to the vault crystal structure (19), the identified P6 peptide adducts (*SI Appendix*, Fig. S4) were mapped within the shoulder (residues 445 to 461) and cap (residues 724 to 734) region of MVP, in agreement with our in silico docking simulation of the C12 vault complex (Fig. 1*D*, a panel on the right). Interestingly, these results suggest C12 localization near MVP domains that could also be involved in interactions with lipid rafts (LRs) (16, 19).

Previous studies on human airway epithelial cells revealed that MVP is recruited to LRs in response to *Pseudomonas aeruginosa*, and activation of the MVP translocation appears to depend on the integrity of LPS, although a role of other bacterial metabolites in this cellular process remains unclear (20). To assess whether C12 is also required for the induction of LR-localized MVP (rMVP), we compared the subcellular localization of MVP in NHBE cells treated with wild-type *P. aeruginosa* or an isogenic mutant strain lacking *lasI*, the gene responsible for the synthesis of C12 (21). A strong and rapid increase in rMVP was evident in response to wild-type bacteria; however, we found a substantial reduction in rMVP when cells were treated with C12-deficient bacteria (Fig. 2*A*). Of note, the residual levels of rMVP observed in response to C12-deficient *P. aeruginosa* could be due to activities of other bacterial stimuli, such as LPS (20) or its essential core component, Kdo_2-lipid A (KLA) (*SI Appendix*, Fig. S5).

To clarify the specific role for C12 in MVP recruitment into LR fractions, we examined induction of rMVP in NHBE cells treated with the natural *S*- or unnatural *R*-stereoisomer of C12 (*SI Appendix*, Fig. S6 *A* and *B*). The subcellular localization of the poly(ADP ribose) polymerase type 4 (PARP4), a component of vaults (22), was also tested. Similar patterns of LR localization were observed for both components of vaults in response to C12 with natural stereochemistry, whereas the unnatural enantiomer was completely inactive (Fig. 2*B*). The induction of LR-localized vault components was not limited to NHBE cells but was also observed in the human lung cancer cell line A549 (Fig. 2*C*) and normal human cord blood-derived macrophages (Fig. 2*D*) treated with C12. The lipophilicity of C12 and other long chain AHLs allows for direct interaction with the plasma membrane (23, 24), and thus, the observed recruitment of the vault components into lipid-rich membrane rafts in response to AHLs (*SI Appendix*, Fig. S6 *C–E*) is consistent with the hypothesis that mammalian sensing of AHLs occurs within a membrane-located system (23).

Observations that C12 activates apoptotic signaling in various cell types and that MVP modulates cancer cell resistance to proapoptotic anticancer agents (13, 25) prompted us to investigate biochemical features relevant to apoptotic effects of C12 and its ability to induce rMVP in lung cancer cell line A549. Western blot (WB) analysis revealed that C12-induced activation of apoptotic caspases and the recruitment of vault components into a LR fraction occurred with similar kinetics; notably, only caspase-8 (casp8) was translocated into LR fractions in response to C12 (Fig. 3*A*), strictly resembling the previously reported process activation of this initiator caspase in cancer cells responding to TRAIL (26). Interestingly, the recruitment of casp8 into LR fractions was equally induced by C12 in both wild-type and MVP-deficient bone marrow-derived macrophages (BMDM) (Fig. 3*B*), suggesting that the observed translocation of vault components and casp8 are two independent events mediated in response to the AHL.

To elucidate whether MVP is involved in the regulation of C12-induced apoptotic signaling, we used cells from wild-type and MVP knockout mice. Titration experiments showed that the viability of BMDM as well as mouse embryonic fibroblasts (MEF) derived from MVP-deficient mice was substantially reduced in the presence of C12 when compared to their wild-type counterparts (*SI Appendix*, Fig. S7*A*), suggesting that MVP contributes to protection against C12-induced cell death. We also observed that the cleavage of poly(ADP ribose) polymerase (PARP) and the activation of caspase-3, two indicative features of apoptosis (27), were faster and more robust in MVP-deficient cells of both types when compared to their wild-type counterparts (Fig. 3 *C* and *D* and *SI Appendix*, Fig. S7*B*). The MVP dependency of C12-mediated responses was specific to apoptotic signaling because the phosphorylation of the eukaryotic translation initiation factor 2 alpha (p-eIF2α) and the splicing of *XbpI* messenger RNA (mRNA), indicative markers of the adaptive endoplasmic reticulum (ER) stress pathway, displayed similar patterns in C12-activated, MVP-deficient, and wild-type cells (Fig. 3 *C* and *D* and *SI Appendix*, Fig. S7*C*).

Apoptosis is initiated through two distinct signaling pathways: the intrinsic pathway, triggered by the effector caspase-9 (casp9), and the extrinsic pathway, that relies on the effector casp8 (27). Although C12 activates both effector caspases (Fig. 3*A*), questions concerning the MVP dependency of this response still needed to be addressed to explain the observed differences in the sensitivity of MVP-deficient and wild-type cells to C12. We found that MVP deficiency substantially increased C12-induced activity of casp8, whereas the induction of casp9 was independent of MVP (Fig. 3 *E* and *F*). Other AHLs revealed similar MVP dependency in activation of apoptotic signaling (*SI Appendix*, Fig. S8*A*). In additional experiments, inflammatory stimuli, such as LPS and KLA, were also tested as controls. Consistent with the ability of both inflammatory stimuli to induce antiapoptotic responses via activation of the NF-κB pathway (6, 9), LPS as well as KLA did not induce apoptotic signaling in either wild-type or MVP-deficient cells (*SI Appendix*, Fig. S8*B*). Thus, this set of findings suggests an essential role for a vault in protection against C12-induced apoptosis exerted through a casp8-dependent mechanism. It also may explain chemoresistance associated with MVP up-regulation in cancer cells (13, 25).

Like LPS, C12 activates the p38 protein kinase pathway that negatively regulates apoptosis in LPS-activated cells (28). However, while LPS also induces inflammatory responses in macrophages through the activation of NF-κB signaling (6), C12 does not. Instead, C12 manifests TLR4-independent anti-inflammatory activity through the inhibition of LPS-mediated transcriptional induction of NF-κB target genes encoding TNF and other inflammatory modulators (11). We found that MVP deficiency had no effect on the induction of TNF and interleukin-1beta (IL-1β) expression in LPS-activated macrophages (Fig. 4*A*, lines in which cells were treated with LPS alone). Additionally, MVP appears dispensable for the anti-inflammatory activity of C12, as LPS-induced TNF production was strongly and equally inhibited by

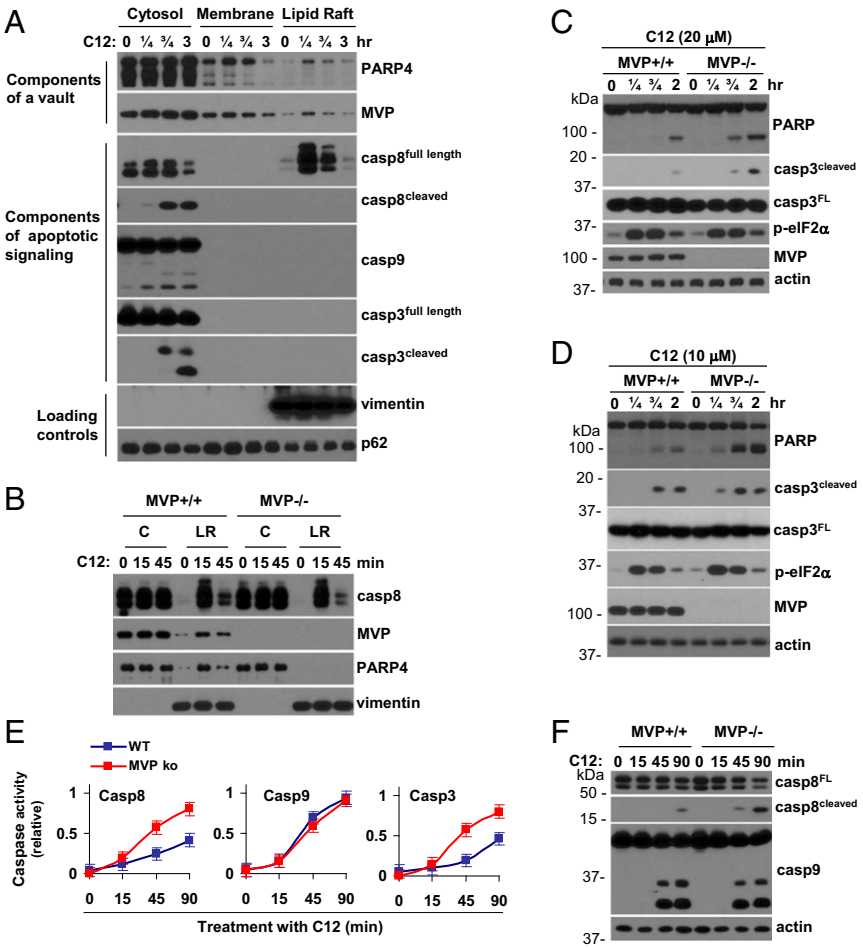

Fig. 3. MVP attenuates C12-induced apoptotic signaling. (*A*) A549 cells were stimulated with C12, and the subcellular fractions were prepared and analyzed by WB for expression of vault components, apoptotic caspases, and loading control markers as indicated. (*B*) BMDM from wild-type ($MVP^{+/+}$) and MVP-deficient ($MVP^{-/-}$) mice were treated with C12 as indicated, and the subcellular fractions (cytosolic [C] and LR) were analyzed by WB for expression of casp8, vault components (MVP and PARP4), and vimentin. (*C*, *D*) WB analysis monitoring PARP and casp3 cleavage as well as the phosphorylation of eIF2α (p-eIF2α) in extracts from wild-type and MVP-deficient MEF (*C*) or BMDM (*D*) stimulated with C12 as indicated. (*E*) Profiles of casp8, casp9, or casp3 activity in BMDM treated with C12. (*F*) WB analysis monitoring activation of initiator caspases (casp8 and casp9) in extracts from $MVP^{+/+}$ or $MVP^{-/-}$ BMDM treated with C12 as indicated. For additional information relevant to experiments described above, see *SI Appendix*, Figs. S7 and S8.

C12 in both wild-type and MVP-deficient BMDM (Fig. 4 *A* and *B*). However, while inflammatory stimuli such as LPS and TNF induced comparable profiles of p38 phosphorylation (p-p38) in wild-type and MVP-deficient cells (*SI Appendix*, Fig. S9), C12-induced p-p38 was substantially impaired in MVP-deficient BMDM and MEF (Fig. 4*C*). In contrast, the C12-mediated effect on the phosphorylation status of other MAPKs, such as JNK and ERK, was similar in wild-type and MVP-deficient macrophages (see WB results for p-JNK and p-ERK1/2 on Fig. 4*C*). Currently, it is unclear whether MVP is directly involved in C12-induced p38 activation or whether MVP/vault, acting as a transporter of signaling components (29, 30), affects expression of p38 within intracellular compartments. Interestingly, WB analysis for p38 and JNK expression in cytoplasmic and LR fractions revealed that cytoplasmic expression of both proteins was unaffected in MVP-deficient macrophages; however, whereas expression of JNK was limited to cytoplasm, p38 was also detected in LR fractions, and levels of the LR-expressed p38 were substantially reduced in MVP-deficient cells (Fig. 4*D*). We also noticed a similarity in responses of MVP- and p38-deficient cells to C12-induced apoptotic signaling (Fig. 4 *E* and *F*; see also *SI Appendix*, Fig. S10), suggesting a role for the MVP-p38 axis in cell survival, for example, in macrophages activated by stimuli other than C12 or a combination of different ones (30, 31).

Integrity of either NF-κB or p38 signaling pathways is essential for macrophage protection against pathogen- or inflammatory stimulus-induced apoptosis (28, 32, 33). In TLR4-activated murine macrophages, proapoptotic immunosurveillance signaling is mitigated by the survival activity of the IKKβ-NF-κB module and p38-mediated phosphorylation-dependent activation of the transcription factor CREB (33). Observations that CREB phosphorylation is seen upon C12 addition to TLR4 ligand-pretreated macrophages (34) prompted us to examine whether C12 alone could activate CREB in human cord blood-derived macrophages (CBM). We observed that C12 induced strong phosphorylation of CREB, which was coincided with activation of p38 but impaired when CBM were pretreated with small interfering RNA (siRNA)-targeting MVP (Fig. 4*G*); also, the reduction of MVP expression compromised CBM survival (Fig. 4 *G*, *Bottom*). It could be relevant to previously reported observations that the MVP-p38 axis is involved in the macrophage scavenger receptor 1 (MSR1)-mediated production of the immunosurveillance cytokine TNF and regulation of apoptotic signaling in macrophage-like cell line RAW264.7 activated by fucoidan, a ligand of MSR1 (29).

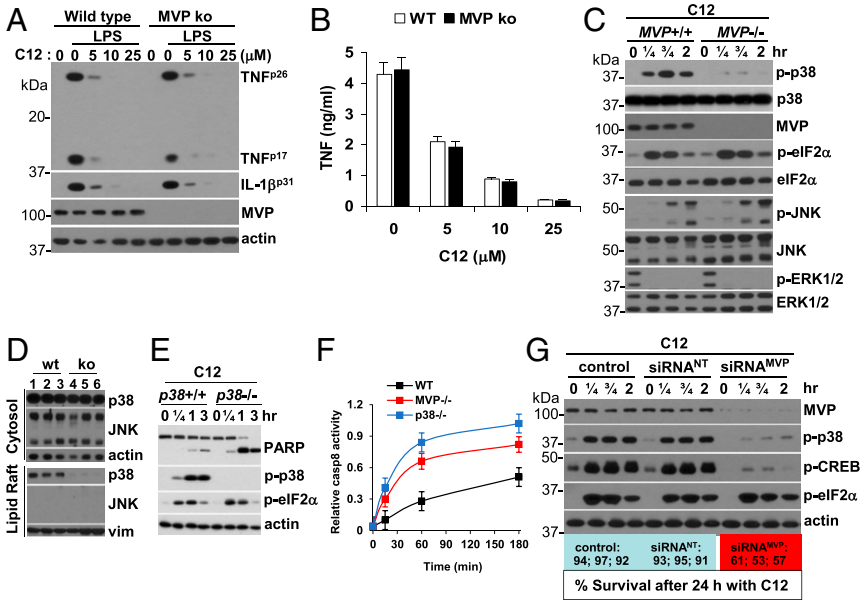

Fig. 4. MVP deficiency selectively affects C12-induced prosurvival activity of p38 signaling. (*A*) WB analysis monitoring expression of TNF and interleukin 1 beta (IL-1β) in extracts from wild-type (WT) and MVP-deficient BMDM stimulated with LPS in the presence of indicated doses of C12. (*B*) TNF secretion from WT or MVP-deficient (MVP ko) BMDM stimulated with LPS in the presence of indicated doses of C12. (*C*) WB analysis for p38, eIF2α, JNK, ERK1/2, and their phosphorylated form as well as MVP in extracts from WT and MVP-deficient BMDM stimulated with C12 as indicated. (*D*) Three independent cytosol and LR fractions from WT (1 to 3) or MVP-deficient BMDM (ko; 4 to 6) were analyzed for expression of p38, JNK, and loading control (vim, an abbreviation for vimentin). (*E*) WB analysis of PARP, p-p38, p-eIF2α, and actin in cellular extracts from WT and p38-deficient cells stimulated by C12. (*F*) Comparison of casp8 activity in WT and MVP- or p38-deficient cells stimulated with C12 (10 mM) as indicated. (*G*) After transfection with MVP-specific siRNA (MVP) or nontargeting control siRNA (NT), untransfected (control) and siRNA-transfected human CBM were treated with C12 for indicated times, and cellular extracts were analyzed by WB for MVP, p-p38, p-CREB, p-eIF2α, and actin. The same set of CBM were also incubated with C12 for 24 h, and cell viability was measured and shown (the bottom boxes; three biological replicates) as a percentage of viable (100%) untreated cells.

Death receptors, such as TNF receptor type 1 (TNFR1) and TRAIL receptor type 2 (also called DR5), regulate immunosurveillance processes through ligand-induced activation of apoptosis in nascent cancer cells (2–9). Since interaction of C12 with the plasma membrane (23, 24) results in TNF-independent activation of TNFR1-mediated apoptotic signaling (24), we examined the subcellular localization of TNFR1, TRADD (TNF receptor-associated death domain), DR5, the apoptotic adaptor protein FADD, caspase-8, and the vault components in CBM simulated by C12 or TNF. In keeping in mind that MSR1 has been identified as a binding partner for MVP (29), analyzing the localization of MSR1 was also included in these studies. WB analysis of subcellular fractions from C12- or TNF-stimulated cells revealed that both stimuli-induced rapid recruitment of vault components (MVP and PARP4) and MSR1 into LR fractions (Fig. 5*A*). We also found that although low levels of LR-localized TNFR1 and DR5 were detected in response to TNF, C12 treatment substantially increased recruitment of both death receptors into LR fractions, in which the presence of TRADD, FADD, and caspase-8 was also evident (Fig. 5*B*). Interestingly, the similarity between patterns of DR5 and MSR1 localization in cytoplasmic fractions was reproducibly observed at late time points after C12 stimulation (Fig. 5 *A* and *B*), which could be relevant to C12-induced ER stress response (35) and TRAIL-independent, DR5-mediated apoptosis (36).

C12 is exclusively produced in certain Gram-negative bacteria that also possess LPS as a key effector of inflammatory and immunosurveillance macrophage responses. Therefore, we examined a subcellular localization of MSR1, vault components, and death receptor signaling partners in LPS-simulated CBM. The results of this analysis shown in Fig. 5*C* revealed that vault components (MVP and PARP4) and MSR1 were rapidly recruited into LR in response to LPS, whereas the localization of casp8, death receptors (DR5 and TNFR1), and FADD was unaffected and consistent with LPS-induced endogenous expression of TNF proteins (TNF p26 and TNF p17); changes in a pattern of TNFR1 expression were coincided with TRADD recruitment into membrane fractions. Thus, like C12 or TNF, cells respond to LPS with translocation of vault components and MSR1 into LR fractions, indicating that the LR-recruitment of MVP-MSR1 composites is a consequence of common processes triggered within the plasma membrane in response to these obviously distinct stimuli.

Within the plasma membrane, LRs are an assemblage of cholesterol, sphingolipids, and proteins, which can be coalesced—by lipid- and/or protein-mediated signaling, such as lipid content/structure alteration, multivalent ligand binding, or protein oligomerization—to raft platforms that are bioactive in cell membrane functions (37). For example, a conversion of sphingomyelin (SM) to ceramide (Cer) triggered in response to inflammatory mediators, such as LPS, and immunosurveillance cytokines, such as TNF and TRAIL, results in formation of Cer-rich raft platforms that regulate anti- and proapoptotic cellular processes essential for cell growth and death (38–42). Of note, Cer induces cell death (43), but it can also be hydrolyzed to fatty acid and sphingosine (Sph), and then, through the sphingolipid salvage pathway (42), acylation of Sph recycles Cer that further can be metabolized to SM; thus, the restored homeostatic balance of lipids within the plasma membrane accompanied with the antiapoptotic effect of NF-κB signaling promotes survival of LPS- or TNF-activated cells (42, 44). On the other hand, C12 inhibits TNF-mediated activation of NF-κB signaling (34) but activates apoptosis through TNFR1 oligomerization (24) and coincided with recruitment of TNFR1/DR5, its apoptotic adaptors, and casp8 into LRs (Fig. 5*B*). These findings suggest that lipophilic interaction of C12 with the plasma membrane promotes Cer-rich raft platform formation, but similar interaction with the ER membrane, where de novo synthesis of Cer

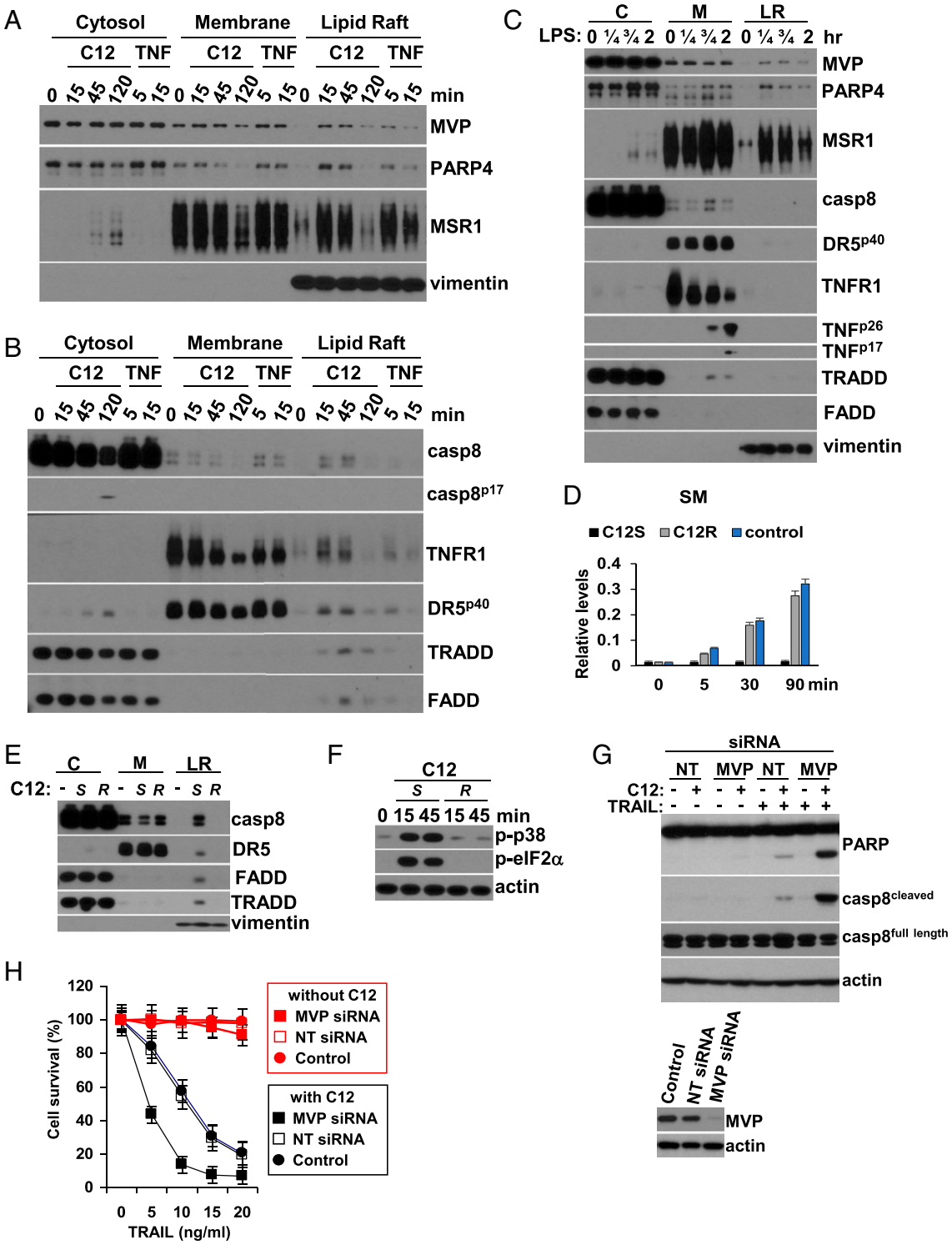

Fig. 5. MVP recruitment into LR platforms could regulate immunoediting and immunosurveillance processes. (*A*) WB analysis monitors expression of the vault components (MVP and PARP4), MSR1, and vimentin in subfractions from CBM stimulated by C12 or TNF as indicated. (*B*) Subtractions shown in *A* were additionally analyzed for expression of the indicated proteins. (*C*) Subfractions (C [cytosol], M [membrane], and LR) were prepared from LPS-stimulated CBM and analyzed for expression of the indicated proteins. (*D*) Relative levels of radioactivity incorporated into sphingomyelin (SM) after 3H-Sph metabolic labeling macrophages treated for different period of time with natural (C12S) or unnatural (C12R) enantiomers of C12; the samples from untreated cells were used as a control. For additional information, please see *SI Appendix*, Fig. S9. (*E* and *F*) CBM were stimulated with *S*- or *R*-enantiomers of C12, and the prepared subfractions (at 30 min after stimulation) were analyzed for expression indicated on a panel of proteins (*E*); in parallel, total cellular extracts were analyzed for expression of the phosphorylated forms of p38 or eIF2α and actin as a loading control (*F*). (*G*) After transfection by MVP-specific siRNA (MVP) or a nontargeting control siRNA (NT), A549 cells treated with C12 (5 μM), TRAIL (10 ng/mL), or a combination of both stimuli for 3 h and cellular extracts were analyzed by WB for PARP and casp8 cleavage as well as for a full length of casp8 and actin as indicated. Silencing of MVP expression in these cells was also verified by WB for MVP (insert on the bottom). (*H*) The same set of A549 transfected cells were incubated with or without C12 (5 μM) in the presence of indicated doses of TRAIL for 18 h, and cell survival was assessed.

occurs (45), could affect the sphingolipid salvage pathway. Although further investigations are required to define mechanisms, our ^{3}H-Sph metabolic labeling experiments on macrophages revealed that addition of C12 substantially impaired ^{3}H-Sph incorporation into Cer and especially SM (Fig. 5*D* and *SI Appendix*, Fig. S11 *A–C*). These findings suggest that C12 interactions with the plasma membrane disrupt metabolically balanced sphingolipid compositions that elicit activation of protein-mediated signaling. Notably, the natural stereochemistry of C12 is required for the modulation of sphingolipid metabolism (*SI Appendix*, Fig. S11*B*) and recruitment of protein-contained apoptotic machinery of death receptors and casp8 into LR platforms as well as for C12-induced activation of p38 and ER stress-mediated phosphorylation of eIF2α (Fig. 5 *E* and *F*). Importantly, consistent with our earlier observations on NHBE cells, the translocation of vault components (MVP and PARP4) into LR fractions was also induced in CBM stimulated only by the natural *S*-enantiomer of C12 (*SI Appendix*, Fig. S11*D*), further supporting specific recognition of C12 by MVP vaults.

The elevated MVP expression in cancer cells correlates with resistance to anticancer therapeutic treatments (30, 46), suggesting a role for the vaults in immunoediting/immunosurveillance processes. Of note, lung cancer A549 cells express high levels of MVP (46) and show resistance to apoptosis induced by the immunosurveillance cytokine TRAIL (7), but C12 restores the sensitivity of tumor cells to TRAIL (10). This effect of C12 on TRAIL activity against cancer cells could be relevant to disruption of sphingolipid metabolism because the apoptotic response to TRAIL+C12 was blocked by D-MAPP, an inhibitor of Cer metabolism (47), whereas bortezomib-mediated effect on TRAIL-induced apoptosis was unaffected by D-MAPP (*SI Appendix*, Fig. S11*E*); also, D-MAPP blocked C12-induced signaling, whereas responses to LPS were unaffected (*SI Appendix*, Fig. S11 *F* and *G*). Having identified the MVP vault as an anti-apoptotic effector of C12, we examined whether MVP is involved in A549 cell resistance to TRAIL. As expected, apoptotic signaling in control siRNA-transfected A549 cells was slightly increased in response to a combination of TRAIL and C12, whereas siRNA-mediated reduction of MVP expression resulted in substantial enhancement of apoptotic signaling (Fig. 5*G*). Titration experiments confirmed that MVP-specific siRNA-targeted cells were more sensitive to TRAIL (Fig. 5*H*). Thus, the observed MVP involvement in TRAIL-induced apoptosis in lung cancer cells may indeed regulate cancer immunoediting/immunosurveillance processes, especially upon *P. aeruginosa* infections.

Our findings suggest a specific function for MVP vaults in the recognition of C12 and other AHLs as indicative signals for the presence of AHL-producing proteobacteria, such as *P. aeruginosa*. Through acting in concert with a TLR4-dependent response to LPS (3, 6, 9, 28), vaults could contribute to survival of activated cells, thereby coupling processes of host immunosurveillance (2, 9, 10) (*SI Appendix*, Fig. S11*C*) and pathogen elimination (20, 48) with resolution of cellular responses to classical inflammatory stimuli including TNF. Therefore, further investigation is warranted into the structure–activity relationships between components of vaults for their therapeutic potential against inflammation-mediated pathologies, including cancer.

Methods

General Methods and Reagents. All chemical reagents for organic synthesis were purchased from Sigma-Aldrich or Acros (Thermo Fisher Scientific) and used without further purification. Solvents were dried with an MBraun solvent purification system. Reactions were monitored by thin-layer chromatography (TLC) using commercially available glass plates precoated with silica (0.25 mm, Merck 60 F254), which were developed using potassium permanganate. Flash chromatography was performed on Merck 40 to 63 μm silica gel. NMR analyses were performed using a Bruker Avance DPX400 or DMX500. Spectra were calibrated on residual solvent signal. All AHLs, including C12 and C12*R*, were synthesized following published procedures (49–51). The synthesis of P6 was previously described (52). The purity of all compounds' purity was confirmed by liquid chromatography–mass spectroscopy (LC–MS) and NMR analysis. In addition, a quantitative QCL-1000 Chromogenic Limulus Amoebocyte Lysate Assay (BioWhittaker, Inc.) demonstrated that preparations of C12 and other AHLs were endotoxin free. [3-^{3}H]-D-erythro-sphingosine (20 Ci/mmol) was obtained from American Radiolabeled Chemicals, Inc. Sphingolipids (Cer, Sph, SP1, DMS, and other lipids) were obtained from Matreaya. In general, synthetic molecules were dissolved in dimethyl sulfoxide (DMSO) or ethanol at 200× of the desired concentration, and aliquots were stored at −20 °C. LPS (*Escherichia coli* serotype 055:B5) was purchased from Sigma-Aldrich while *Salmonella minnesota* Re595 LPS was prepared as previously described (53). The core structural component of LPS, also referred to Di[3-deoxy-D-manno-octulosonyl]-lipid A, Kdo_2-Lipid A, or KLA, was obtained from Avanti. Supernatant levels of TNF or IL-6 in the samples were measured by enzyme-linked immunosorbent assay (BD Biosciences Pharmingen).

Live-Cell Labeling with Diazirine Analog Probes. Cells were plated at 20% confluence in culture medium and grown to approximately 90% confluency. Stock solutions of the probes and the C12 were dissolved in DMSO. Medium was replaced 12 h prior to the experiment. Compounds were added to a concentration indicated in figure legends, and the cells were incubated for 30 min. The cells were washed once with cold phosphate-buffered saline (PBS) and UV irradiated for 15 min on a UV table at 365 nm at 4 °C. Cells were collected using a cell scraper, and stored at −80 °C. For SILAC experiments, labeling was performed in a similar manner, but the cells were grown in SILAC Dulbecco's Modified Eagle Medium (DMEM) and dialyzed fetal bovine serum (FBS) purchased from Biological Industries complemented with isotopically enriched arginine and lysine for the heavy medium, or with the same light amino acids, all purchased from Sigma-Aldrich.

CuAAC Chemistry for In-Gel Visualization. CuAAC chemistry was performed based on protocols from the Cravatt Laboratory (54). The protein concentration of each sample was measured using a bicinchoninic acid BCA protein assay (Pierce BCA Protein Assay Kit; Thermo Fisher Scientific) and normalized by dilution with PBS to approximately 1 to 3 mg/mL. For each sample, 1 mL proteome was taken, and the following reagents were added: rhodamine azide (10 μL 10 mM in DMSO, final concentration: 100 μM); tris(2-carboxyethyl)phosphine (TCEP; 20 μL 50 mM in PBS, prepared fresh, final concentration: 1 mM); tris[(1-benzyl-1H-1,2,3-triazol-4-yl)methyl]amine (60 μL 1.7 mM in 1:4 DMSO:t-butanol, final concentration: 100 μM); $CuSO_4$ (20 μL 50 mM in double-distilled water [DDW], final concentration: 2 mM). The mixture was allowed to react for 1 h at room temperature on a shaker. Lastly, the samples were analyzed by sodium dodecyl sulfate (SDS)-polyacrylamide gel electrophoresis gel, and the gel was visualized using an ImageQuant LAS 4000 Imager (Fujifilm) set in Cy3 fluorescence mode (excitation/emission = 520 nm/575 nm).

CuAAC Protocol and Sample Preparation for Proteomics Analysis. Sample preparation was performed based on protocols from the Cravatt Laboratory (54). For SILAC samples, the heavy and light proteomes were combined in a 1:1 ratio before proceeding. CuAAC chemistry was performed as described above, using biotin azide instead of rhodamine azide. Excess reagents were removed using methanol/chloroform (MeOH/$CHCl_3$) precipitation: the samples were transferred to 15 mL conical tubes on ice, 2 mL cold MeOH was added, 0.5 mL cold $CHCl_3$ was added, and the sample was vortexed. Next, 1.0 mL cold PBS was added and the sample was vortexed and centrifuged at 5,000 rpm for 10 min. The top and bottom layers were removed, leaving the protein interface, and the sample was washed with 1:1 MeOH:$CHCl_3$ (1.0 mL, 3×). 2 mL of MeOH was added and the sample was sonicated with a probe sonicator, and then 0.5 mL $CHCl_3$ was added. Lastly, the sample was centrifuged at 5,000 rpm for 10 min to pellet protein and the supernatant was removed. Next, the samples were denatured and reduced: 500 μL 6M urea (in PBS, made fresh) and 50 μL premixed 100 mM TCEP/300 mM K_2CO_3 solution (in PBS) were added and the sample was sonicated and incubated for 30 min at 37 °C in shaker. Next, 70 μL 400 mM iodoacetic acid was added and incubated for 30 min at room temperature in the dark, 140 μL 10% SDS in PBS was added, and the sample was diluted with 5.5 mL PBS.

Enrichment and Trypsinization for Proteomics Analysis. Enrichment and trypsinization was performed based on protocols from the Cravatt Laboratory (54). Enrichment was performed as follows: Sample was added to 100 μL of Streptavidin beads (beads were washed 3× with 500 μL PBS) and incubated 1.5 h at room temperature on shaker. The sample was centrifuged to pellet beads, and the beads were washed 3×, each of 10 mL 0.2% SDS/PBS, PBS, and DDW. Lastly, the beads were transferred to low-binding Eppendorf

tubes using 2× 0.5 mL DDW and spun down, and then the supernatant was removed. Trypsinization was performed as follows. The following reagents were premixed and then added to each tube: 200 μL 2M urea/PBS, 2 μL 100 mM $CaCl_2$, and 4 μL Trypsin (20 μg reconstituted in 40 μL Trypsin buffer). The tubes were shaken overnight (up to 12 h) at 37 °C. The beads were then pelleted by a brief centrifugation, and the supernatant and beads were transferred to a small spin column, and the supernatant was collected by centrifugation. The beads were washed with 100 μL PBS and collected in the same tube. The filtrate was acidified using 16 μL formic acid and stored at −20 °C.

Proteomics MS Analysis. Samples were analyzed using an LTQ Orbitrap XL ETD (Thermo Fisher Scientific) coupled to a NanoLC-2D (Eksigent), and proteins were identified with ProLuCID (55), using parameters as previously reported (56). SILAC ratio was calculated using CImage (57). Full SILAC results are available in the MassIVE database under accession number MSV000084474 (https://doi.org/doi:10.25345/C5P95Q) (58).

Labeling of Purified Vaults. Purified human recombinant vaults were prepared following previously reported procedures (18). For labeling experiments, 1 μM vaults were incubated with varying concentrations of P6 (1, 5, or 10 μM) with or without C12 (1 to 100 μM) for half an hour on a shaker. Labeling, CuAAC chemistry, and in-gel visualization were performed as described above.

Docking Studies. C12 structure extracted from the Protein Data Bank (PDB) 3IX3 was docked onto an MVP chain from the vault crystal structure (PDB 4v60) with a blind docking method using Binding Site Prediction with Shape-based LIgand Matching (BSP-SLIM) (https://zhanglab.ccmb.med.umich.edu/BSP-SLIM/) (59). Data were analyzed and figures were generated using PyMOL.

Cleavable Levulinic Linker Synthesis. The linker was synthesized according to the scheme shown in *SI Appendix*, Fig. S12. First, 4-oxonon-8-ynoic acid was synthesized as previously reported (52). To a solution of 4-oxonon-8-ynoic acid (504 mg, 3 mmol) and 1,2-bis(2-azidoethoxy) (6 g, 10 eq., 30 mmol) in dimethylformamide (DMF):H_2O (9:1, 30 mL), CuCl (94 mg, 0.2 eq., 0.6 mmol) and sodium ascorbate (178 mg, 10.3 eq., 0.9 mmol) were added, and the mixture was stirred overnight at room temperature. The mixture was filtered through a short pad of celite and was used without further purification. The crude acid, biotin-ethanolamine (862 mg, 3 mmol), N-hydroxysuccinimide (345 mg, 3 mmol), and 4-dimethylaminopyridine (36 mg, 0.3 mmol) were dissolved in DMF (30 mL). The carbodiimide 1-ethyl-3-(3-dimethylaminopropyl)carbodiimide (747 mg, 3.9 mmol) was added portion wise, and the mixture was stirred for 14 h. Finally, it was concentrated under reduced pressure, and the title compound was obtained after reversed-phase high-performance liquid chromatography purification (10% → 90% MeCN/0.1% TFA).

NMR spectra are shown in *SI Appendix*, Fig. S13; ^{1}H NMR (400 MHz, DMSO): δ 1.21 to 1.40 (m, 2H), 1.40 to 1.69 (m, 4H), 1.79 (quint., J = 7.4 Hz, 2H), 2.07 (t, J = 7.3 Hz, 2H), 2.54 to 2.63 (m, 3H), 2.69 (t, J = 6.4 Hz, 2H), 2.82 (dd, J = 5 Hz, 12.4 Hz, 1H), 3.06 to 3.13 (m, 1H), 3.26 (quad, J = 5.5 Hz, 2H), 3.37 (m, 3H), 3.52 to 3.58 (m, 6H), 3.81 (t, J = 5 Hz, 3H), 3.98 (t, J = 5.6 Hz, 2H), 4.13 (m, 1H), 4.31 (m, 1H), 4.47 (t, J = 5 Hz, 2H), 6.42 (s, 1H), 6.36 (s, 1H), 7.82 (s, 1H), and 7.09 (t, J = 5.5 Hz, 1H); ^{13}C NMR (100 MHz, $CDCl_3$): δ 23.6, 24.8, 25.6, 28, 28.5, 28.6, 35.5, 37, 37.9, 41.5, 49.7, 50.4, 55.8, 59.6, 61.5, 63.1, 69.2, 69.6, 70, 70, 122.7, 146.7, 163.2, 172.7, 172.8, and 209.1.

Cleavable Levulinic Linker Model Cleavage Reaction. To verify that this labeling method is feasible, the cleavable levulinic linker was incubated overnight with 50 mM of heavy (^{15}N) and light (^{14}N) hydrazine at pH 7.5, and the reaction was analyzed by LC–MS. Only two major products were detected: dihydropyridazin-3-one and biotin aminoethanol. The desired dihydropyridazin-3-one showed the expected doublet profile for the heavy and light cleavage showing incorporation of two ^{15}N atoms into the product, with peaks detected at 365.31 *m/z* and 367.28 *m/z* (predicted mass + H: 365.19 and 367.19 *m/z* for heavy and light, respectively).

MS Analysis of Purified Vaults. The CuAAC reactions were performed as above for biotinylation of 1 μM purified vaults using a cleavable levulinic linker (100 μM). The enrichment and trypsin digest were performed as described above, without the chloroform/methanol precipitation steps. Data analysis was performed as detailed above, and then the labeled peptides were identified using a custom Python script, which searched for heavy and light labeled peptides of a similar intensity (at least 80% similarity) within 2-min retention time windows. The script is available at https://github.com/barashe/levulinic_linker (60).

Mice, BMDM, and Other Cells. C57BL/6 mice were purchased from the Jackson Laboratory. MVP-deficient mice and littermate controls (all mice were of the C57BL/6 background) were described previously (61). BMDM and MEF were prepared by using standard protocols. MEFs deficient in p38α were obtained from p38α loxp/loxp mice and immortalized with a retrovirus expressing the large T antigen. The p38α loxp/loxp mice were kindly provided by Huiping Jiang, Boehringer Ingelheim Pharmaceuticals, Inc., Ridgefield, CT. NHBE were obtained from Cambrex and cultured as recommended by the manufacturer. Lung cancer epithelial cell line A549 was purchased from the American Type Culture Collection (ATCC). Normal human CD34$^+$ cord blood cells obtained from StemCell Technologies were cultured as recommended by the manufacturer and used for preparation of normal human CBM as previously described (62). MEF and cell lines were maintained in the following growth medium (GM): DMEM (4.5 g/L glucose) supplemented with 10% FBS (HyClone Laboratories, Inc.), *L*-glutamine, penicillin/streptomycin, and nonessential amino acids (Invitrogen). BMDM were cultured in 70% GM and 30% L929 conditioned medium. In general, cells (~60 to 70% confluence) were incubated in corresponding fresh medium for 12 to 14 h before stimulation.

Exposure of NHBE Cells to Bacteria. The *P. aeruginosa* bacteria used in our studies were kindly provided by Scott A. Beatson, University of Queensland, Brisbane, Australia, and include wild-type *P. aeruginosa* PAO1 (originally from ATCC) and PAO1 Δ*lasI*. The bacteria were grown on brain heart infusion (BHI) agar plates and then transferred to inoculum culture overnight, followed by 1/100 dilution into 20 mL BHI broth in 125 mL baffled shake flasks for incubation at 37 °C, 250 rpm for 4 to 6 h. The equal aliquots of the late log phase culture or control BHI broth were transferred to PVDF inserts, which were placed in 24-well plates containing target cells cultured in 0.5 mL GM as previously described (34).

Determination of C12 Concentration in Bacterial Cultures. A total of 2 mL bacterial culture was acidified with 50 μL HCl and 10 mL ethyl acetate was added, and the contents were mixed vigorously. The layers were allowed to separate, and 5 mL of the ethyl acetate layer were removed, dried over $MgSO_4$, and concentrated in vacuo. The residue was resuspended in cold methanol and centrifuged to remove the precipitate. The resulting methanol solution was analyzed by LC–MS for C12 content. Reverse phase LC–MS analysis (Agilent ZORBAX column, 5 μm, 300SB-C8, 4.6 × 50 mm) was performed with gradients of MeCN–H_2O–0.1% formic acid (from 0 to 1 min: 5% MeCN, from 1 min to 9 min: gradient of 5% MeCN to 98% MeCN, and from 9 to 11 min: 98% MeCN), allowing for quantification of C12 by measuring the following ions: 298 (M + H^+), 316 (M + H_2O + H^+), 320 (M + Na^+), and 338 (M + H_2O + Na^+). The concentration of C12 in the samples of *P. aeruginosa* PAO1 (wild type) was about 4.3 μM ($P < 0.001$, $n = 5$ independent experiments). Similar samples from LasI-deficient bacteria as well as from *Staphylococcus aureus* and *Salmonella typhimurium* were C12-negative.

Antibodies and WB Analysis. Antibodies specific for vimentin, HSP70, the full-length caspase-3 (casp3^{FL}), the cleaved form of caspase-3 (casp3^{cleaved}), the full-length caspase-8 (casp8^{FL}), the cleaved form of caspase-8 (casp8^{cleaved}), the full-length caspase-9 (casp9), eIF2α, phospho-eIF2α (p-eIF2α), p38, phospho-p38 (p-p38), MKK3/MKK6, phospo-MKK3, and PARP were purchased from Cell Signaling; anti-actin antibodies were from Sigma; and anti-MVP antibodies and anti-PARP4 were from GeneTex. The cellular extracts were prepared and analyzed by WB as previously described (63).

Cell Stimulation. In all experiments, cells were stimulated with C12 (in a range of 2 to 20 μM), LPS (100 ng/mL), or their combination as indicated in the figure legends; MEF were stimulated with TNF (40 ng/mL) or KLA (50 nM) as indicated in text or figure legends. CBM were stimulated with 10 nM of KLA.

Subcellular Fractionation. ProteoExtract Subcellular Proteome Extraction Kit (Calbiochem, category no. 539790) was used for the differential extraction of proteins according to their subcellular localization. All subcellular fractionation experiments were performed as recommended by the manufacturer.

XBP1 Assay. The XBP1 splicing assay for expression of u*XBP1* or s*XBP1* mRNA was done by using the OneStep RT-PCR Kit from QIAGEN. Primers encompassing the spliced sequences in XPB1 mRNA (mouse: 5′-GGCCTTGTGGTTGAGAACCAGGAG-3′, 5′-GAATGCCCAAAAGGATATCAGACTC-3′; human: 5′- GAACCAGGAGTTAAGACAGC-3′, 5′-AGTCAATACCGCCAGAATCC-3′) were used for RT-

PCR amplification, and products were separated by electrophoresis through 5% polyacrylamide gel on tris-borate or tris-acetate-EDTA buffer and visualized by ethidium bromide staining.

Cell Viability. Since prolonged incubation of cells with high concentration of C12 (50 μM or higher) exerts a cytotoxic effect (35), in our studies we used low concentration of C12 (from 5 to 25 μM for macrophages and 10 to 40 μM for fibroblast and epithelial cells), and the duration of all experiments was limited up to 3 h. Under these conditions, the viability of C12-treated cells was indistinguishable from control cells, as was determined by using an XTT-based Toxicology Assay Kit (Sigma).

Metabolism of [^{3}H]-Sphingosine in Macrophages. Metabolic labeling and analysis of sphingosine metabolism was performed according to the method described by Yatomi et al. (64) with modifications. BMDM were set up in 30 mm dishes (~10^5 cells per dish) and cultured for 2 d. The cells were incubated with 25 nM [^{3}H]-sphingosine (1 μCi) in the presence or absence of 20 μM C12. At the indicated times, the dish was put on ice and washed by cold PBS, and the cells were collected by centrifugation, resuspended in 0.2 mL of ice-cold PBS, and 1.875 mL of mixture containing chloroform/methanol/concentrated HCl (100:200:1) was added. The lipids were extracted from the cell suspensions by the method of Bligh and Dyer (65). The lipids were recovered in a small volume of chloroform/methanol (2:1); the aliquots (about 5,000 cpm per each sample) of lipid fractions were applied to silica gel 60 TLC plates (Merck), and the plates were developed in butanol/acetic acid/water (3:1:1). The appropriate lipid standards were run on the same TLC plate. The bands were identified by staining the control lipids with primulin and following visualization under UV light. After enhancer (EN^{3}HANCE spray, PerkinElmer Life & Analytical Sciences) treatment of the TLC plate, autoradiography was performed with Kodak MS film at −80 °C for 20 to 40 h. In some experiments, the radioactive spots were scraped off and counted by liquid scintillation counting. Each autoradiograph shown is representative of at least three experiments.

Caspase Assay. The activity of caspase-3, caspase-8, and caspase-9 were measured by using caspase assay kits (R&D System) as recommended in manufacturer's protocols.

Statistics. Data depicted in Figs. 1–4 and *SI Appendix*, Figs. S1–S11 represent one of three or more experiments with each graph reflecting findings typical of multiple studies, and the data were expressed as the relative fold increases compared to the values of untreated or control-treated cells (n = 3 to 5).

Data Availability. Full proteomics and SILAC results are available in the MassIVE database under accession number MSV000084474 (58). Python script for the peptide labeling strategy using the levulinic acid linker is available on Github: https://github.com/barashe/levulinic_linker (60).

ACKNOWLEDGMENTS. We thank Jiahuai Han for providing comments on the manuscript. We also thank Mark Karpasas for guidance on the proteomics analysis. The research was supported by grants from the European Research Council (Starting Grant #240356) to M.M.M. and the US–Israel Binational Science Foundation (Grant #2011360) to M.M.M. and B.F.C. R.G. is grateful to the Azrieli Foundation for the award of an Azrieli Fellowship.

1. M. J. Smyth, D. I. Godfrey, J. A. Trapani, A fresh look at tumor immunosurveillance and immunotherapy. *Nat. Immunol.* **2**, 293–299 (2001).
2. G. P. Dunn, L. J. Old, R. D. Schreiber, The immunobiology of cancer immunosurveillance and immunoediting. *Immunity* **21**, 137–148 (2004).
3. Y. Ben-Neriah, M. Karin, Inflammation meets cancer, with NF-κB as the matchmaker. *Nat. Immunol.* **12**, 715–723 (2011).
4. R. J. Moore *et al.*, Mice deficient in tumor necrosis factor-alpha are resistant to skin carcinogenesis. *Nat. Med.* **5**, 828–831 (1999).
5. J. Wilson, F. Balkwill, The role of cytokines in the epithelial cancer microenvironment. *Semin. Cancer Biol.* **12**, 113–120 (2002).
6. A. Hoffmann, D. Baltimore, Circuitry of nuclear factor kappaB signaling. *Immunol. Rev.* **210**, 171–186 (2006).
7. A. Ashkenazi *et al.*, Safety and antitumor activity of recombinant soluble Apo2 ligand. *J. Clin. Invest.* **104**, 155–162 (1999).
8. H. Walczak *et al.*, Tumoricidal activity of tumor necrosis factor-related apoptosis-inducing ligand in vivo. *Nat. Med.* **5**, 157–163 (1999).
9. J. L. Luo, S. Maeda, L. C. Hsu, H. Yagita, M. Karin, Inhibition of NF-kappaB in cancer cells converts inflammation- induced tumor growth mediated by TNFalpha to TRAIL-mediated tumor regression. *Cancer Cell* **6**, 297–305 (2004).
10. V. Kravchenko *et al.*, Facilitating cytokine-mediated cancer cell death by proteobacterial N-acylhomoserine lactones. *ACS Chem. Biol.* **8**, 1117–1120 (2013).
11. V. V. Kravchenko, G. F. Kaufmann, Bacterial inhibition of inflammatory responses via TLR-independent mechanisms. *Cell. Microbiol.* **15**, 527–536 (2013).
12. L. Dubinsky *et al.*, Species selective diazirine positioning in tag-free photoactive quorum sensing probes. *Chem. Commun. (Camb.)* **49**, 5826–5828 (2013).
13. G. L. Scheffer *et al.*, The drug resistance-related protein LRP is the human major vault protein. *Nat. Med.* **1**, 578–582 (1995).
14. S. K. Vasu, N. L. Kedersha, L. H. Rome, cDNA cloning and disruption of the major vault protein alpha gene (mvpA) in Dictyostelium discoideum. *J. Biol. Chem.* **268**, 15356–15360 (1993).
15. V. A. Kickhoefer, L. H. Rome, The sequence of a cDNA encoding the major vault protein from Rattus norvegicus. *Gene* **151**, 257–260 (1994).
16. H. Tanaka, T. Tsukihara, Structural studies of large nucleoprotein particles, vaults. *Proc. Jpn. Acad., Ser. B, Phys. Biol. Sci.* **88**, 416–433 (2012).
17. Y. Mikyas *et al.*, Cryoelectron microscopy imaging of recombinant and tissue derived vaults: Localization of the MVP N termini and VPARP. *J. Mol. Biol.* **344**, 91–105 (2004).
18. A. G. Stephen *et al.*, Assembly of vault-like particles in insect cells expressing only the major vault protein. *J. Biol. Chem.* **276**, 23217–23220 (2001).
19. H. Tanaka *et al.*, The structure of rat liver vault at 3.5 angstrom resolution. *Science* **323**, 384–388 (2009).
20. M. P. Kowalski *et al.*, Host resistance to lung infection mediated by major vault protein in epithelial cells. *Science* **317**, 130–132 (2007).
21. R. S. Smith, B. H. Iglewski, Pseudomonas aeruginosa quorum sensing as a potential antimicrobial target. *J. Clin. Invest.* **112**, 1460–1465 (2003).
22. V. A. Kickhoefer *et al.*, The 193-kD vault protein, VPARP, is a novel poly(ADP-ribose) polymerase. *J. Cell Biol.* **146**, 917–928 (1999).
23. B. M. Davis, R. Jensen, P. Williams, P. O'Shea, The interaction of N-acylhomoserine lactone quorum sensing signaling molecules with biological membranes: Implications for inter-kingdom signaling. *PLoS One* **5**, e13522 (2010).
24. D. Song *et al.*, Pseudomonas aeruginosa quorum-sensing metabolite induces host immune cell death through cell surface lipid domain dissolution. *Nat. Microbiol.* **4**, 97–111 (2019).
25. Y. S. Xiao *et al.*, Major vault protein is a direct target of Notch1 signaling and contributes to chemoresistance in triple-negative breast cancer cells. *Cancer Lett.* **440-441**, 156–167 (2019).
26. Z. Jin *et al.*, Cullin3-based polyubiquitination and p62-dependent aggregation of caspase-8 mediate extrinsic apoptosis signaling. *Cell* **137**, 721–735 (2009).
27. L. Galluzzi *et al.*, Molecular mechanisms of cell death: Recommendations of the nomenclature committee on cell death 2018. *Cell Death Differ.* **25**, 486–541 (2018).
28. J. M. Park, F. R. Greten, Z. W. Li, M. Karin, Macrophage apoptosis by anthrax lethal factor through p38 MAP kinase inhibition. *Science* **297**, 2048–2051 (2002).
29. J. Ben *et al.*, Major vault protein regulates class A scavenger receptor-mediated tumor necrosis factor-α synthesis and apoptosis in macrophages. *J. Biol. Chem.* **288**, 20076–20084 (2013).
30. W. Berger, E. Steiner, M. Grusch, L. Elbling, M. Micksche, Vaults and the major vault protein: Novel roles in signal pathway regulation and immunity. *Cell. Mol. Life Sci.* **66**, 43–61 (2009).
31. P. Moura-Alves *et al.*, Host monitoring of quorum sensing during *Pseudomonas aeruginosa* infection. *Science* **366**, eaaw1629 (2019).
32. L. C. Hsu *et al.*, The protein kinase PKR is required for macrophage apoptosis after activation of Toll-like receptor 4. *Nature* **428**, 341–345 (2004).
33. J. M. Park *et al.*, Signaling pathways and genes that inhibit pathogen-induced macrophage apoptosis—CREB and NF-kappaB as key regulators. *Immunity* **23**, 319–329 (2005).
34. V. V. Kravchenko *et al.*, Modulation of gene expression via disruption of NF-kappaB signaling by a bacterial small molecule. *Science* **321**, 259–263 (2008).
35. V. V. Kravchenko *et al.*, N-(3-oxo-acyl)homoserine lactones signal cell activation through a mechanism distinct from the canonical pathogen-associated molecular pattern recognition receptor pathways. *J. Biol. Chem.* **281**, 28822–28830 (2006).
36. M. Lam, S. A. Marsters, A. Ashkenazi, P. Walter, Misfolded proteins bind and activate death receptor 5 to trigger apoptosis during unresolved endoplasmic reticulum stress. *eLife* **9**, e52291 (2020).
37. D. Lingwood, K. Simons, Lipid rafts as a membrane-organizing principle. *Science* **327**, 46–50 (2010).
38. H. Grassmé *et al.*, Host defense against Pseudomonas aeruginosa requires ceramide-rich membrane rafts. *Nat. Med.* **9**, 322–330 (2003).
39. A. Płóciennikowska, A. Hromada-Judycka, K. Borzęcka, K. Kwiatkowska, Co-operation of TLR4 and raft proteins in LPS-induced pro-inflammatory signaling. *Cell. Mol. Life Sci.* **72**, 557–581 (2015).
40. G. S. Dbaibo, L. M. Obeid, Y. A. Hannun, Tumor necrosis factor-alpha (TNF-alpha) signal transduction through ceramide. Dissociation of growth inhibitory effects of TNF-alpha from activation of nuclear factor-kappa B. *J. Biol. Chem.* **268**, 17762–17766 (1993).
41. C. A. Dumitru, E. Gulbins, TRAIL activates acid sphingomyelinase via a redox mechanism and releases ceramide to trigger apoptosis. *Oncogene* **25**, 5612–5625 (2006).
42. Y. A. Hannun, L. M. Obeid, Principles of bioactive lipid signalling: Lessons from sphingolipids. *Nat. Rev. Mol. Cell Biol.* **9**, 139–150 (2008).
43. L. M. Obeid, C. M. Linardic, L. A. Karolak, Y. A. Hannun, Programmed cell death induced by ceramide. *Science* **259**, 1769–1771 (1993).

44. Q. Zhang, M. J. Lenardo, D. Baltimore, 30 Years of NF-κB: A blossoming of relevance to human pathobiology. *Cell* **168**, 37–57 (2017).
45. A. H. Merrill Jr, De novo sphingolipid biosynthesis: A necessary, but dangerous, pathway. *J. Biol. Chem.* **277**, 25843–25846 (2002).
46. W. Berger, L. Elbling, M. Micksche, Expression of the major vault protein LRP in human non-small-cell lung cancer cells: Activation by short-term exposure to antineoplastic drugs. *Int. J. Cancer* **88**, 293–300 (2000).
47. A. Bielawska *et al*., (1S,2R)-D-erythro-2-(N-myristoylamino)-1-phenyl-1-propanol as an inhibitor of ceramidase. *J. Biol. Chem.* **271**, 12646–12654 (1996).
48. M. W. Marino *et al*., Characterization of tumor necrosis factor-deficient mice. *Proc. Natl. Acad. Sci. U.S.A.* **94**, 8093–8098 (1997).
49. G. F. Kaufmann *et al*., Revisiting quorum sensing: Discovery of additional chemical and biological functions for 3-oxo-N-acylhomoserine lactones. *Proc. Natl. Acad. Sci. U.S.A.* **102**, 309–314 (2005).
50. A. L. Garner *et al*., Synthesis of 'clickable' acylhomoserine lactone quorum sensing probes: Unanticipated effects on mammalian cell activation. *Bioorg. Med. Chem. Lett.* **21**, 2702–2705 (2011).
51. A. L. Garner *et al*., Immunomodulation and the quorum sensing molecule 3-oxo-C12-homoserine lactone: The importance of chemical scaffolding for probe development. *Chem. Commun. (Camb.)* **49**, 1515–1517 (2013).
52. L. Dubinsky *et al*., Synthesis and validation of a probe to identify quorum sensing receptors. *Chem. Commun. (Camb.)*, 7378–7380 (2009).
53. J. C. Mathison *et al*., Adaptation to bacterial lipopolysaccharide controls lipopolysaccharide-induced tumor necrosis factor production in rabbit macrophages. *J. Clin. Invest.* **85**, 1108–1118 (1990).
54. A. E. Speers, B. F. Cravatt, Activity-based protein profiling (ABPP) and click chemistry (CC)-ABPP by MudPIT mass spectrometry. *Curr. Protoc. Chem. Biol.* **1**, 29–41 (2009).
55. T. Xu *et al*., ProLuCID: An improved SEQUEST-like algorithm with enhanced sensitivity and specificity. *J. Proteomics* **129**, 16–24 (2015).
56. M. J. Niphakis *et al*., A global map of lipid-binding proteins and their ligandability in cells. *Cell* **161**, 1668–1680 (2015).
57. E. Weerapana *et al*., Quantitative reactivity profiling predicts functional cysteines in proteomes. *Nature* **468**, 790–795 (2010).
58. M. M. Meijler, MSV000084474: Rayo et al., Immunoediting Role for Major Vault Protein in Apoptotic Signaling Induced by N-Acyl Homoserine Lactones. MassIVE. https://doi.org/doi:10.25345/C5P95Q. Deposited 18 October 2019.
59. H. S. Lee, Y. Zhang, BSP-SLIM: A blind low-resolution ligand-protein docking approach using predicted protein structures. *Proteins* **80**, 93–110 (2012).
60. E. Barash, Levulinic linker code. GitHub. https://github.com/barashe/levulinic_linker. Deposited 22 January 2019.
61. M. H. Mossink *et al*., Disruption of the murine major vault protein (MVP/LRP) gene does not induce hypersensitivity to cytostatics. *Cancer Res.* **62**, 7298–7304 (2002).
62. H. Shi *et al*., NLRP3 activation and mitosis are mutually exclusive events coordinated by NEK7, a new inflammasome component. *Nat. Immunol.* **17**, 250–258 (2016).
63. V. V. Kravchenko, R. J. Ulevitch, G. F. Kaufmann, Modulation of mammalian cell processes by bacterial quorum sensing molecules. *Methods Mol. Biol.* **692**, 133–145 (2011).
64. Y. Yatomi *et al*., N,N-dimethylsphingosine inhibition of sphingosine kinase and sphingosine 1-phosphate activity in human platelets. *Biochemistry* **35**, 626–633 (1996).
65. E. G. Bligh, W. J. Dyer, A rapid method of total lipid extraction and purification. *Can. J. Biochem. Physiol.* **37**, 911–917 (1959).